NASA TECHNICAL NOTE

NASA TN D-6638

HOT-GAS-SIDE HEAT TRANSFER WITH AND WITHOUT FILM COOLING ON A SIMULATED NUCLEAR ROCKET THRUST CHAMBER USING H_2-O_2

by Richard J. Quentmeyer, Ralph L. Schacht, and William L. Jones

Lewis Research Center
Cleveland, Ohio 44135

NATIONAL AERONAUTICS AND SPACE ADMINISTRATION • WASHINGTON, D. C. • FEBRUARY 1972

1. Report No. NASA TN D-6638	2. Government Accession No.	3. Recipient's Catalog No.
4. Title and Subtitle HOT-GAS-SIDE HEAT TRANSFER WITH AND WITHOUT FILM COOLING ON A SIMULATED NUCLEAR ROCKET THRUST CHAMBER USING H_2-O_2		5. Report Date February 1972 6. Performing Organization Code
7. Author(s) Richard J. Quentmeyer, Ralph L. Schacht, and William L. Jones		8. Performing Organization Report No. E-6553
9. Performing Organization Name and Address Lewis Research Center National Aeronautics and Space Administration Cleveland, Ohio 44135		10. Work Unit No. 112-29 11. Contract or Grant No.
12. Sponsoring Agency Name and Address National Aeronautics and Space Administration Washington, D.C. 20546		13. Type of Report and Period Covered Technical Note 14. Sponsoring Agency Code

15. Supplementary Notes

16. Abstract

Heat-transfer coefficients were obtained on a thrust chamber which simulated the geometry of the NERVA nuclear rocket. The tests were performed with and without peripheral film cooling over a chamber pressure range of 105×10^4 to 584×10^4 newtons per square meter (153 to 847 psia). With no film cooling, the overall axial variation in the value of the correlation coefficient C of the equation $(\text{Stanton})^*(\text{Prandtl})^{*.7} = C(\text{Reynolds})^{*-.2}$ was reduced 66 percent when the local diameter in the Reynolds number was replaced by the axial distance from the injector face. The average peak values of C were reduced 25 percent with 2 and 3.75 percent cooling and 50 percent with 7.5 percent cooling.

17. Key Words (Suggested by Author(s))
Convective heat transfer, Heat transfer coefficients, Heat transfer, Nuclear rocket engines, Hydrogen oxygen engines, Film cooling

18. Distribution Statement
Unclassified - unlimited

19. Security Classif. (of this report)	20. Security Classif. (of this page)	21. No. of Pages	22. Price*
Unclassified	Unclassified	38	$3.00

* For sale by the National Technical Information Service, Springfield, Virginia 22151

HOT-GAS-SIDE HEAT TRANSFER WITH AND WITHOUT FILM COOLING ON A SIMULATED NUCLEAR ROCKET THRUST CHAMBER USING H_2-O_2

by Richard J. Quentmeyer, Ralph L. Schacht, and William L. Jones

Lewis Research Center

SUMMARY

Heat-transfer coefficients were obtained on a thrust chamber which simulated the geometry of a NERVA nuclear rocket. The tests were performed using a copper heat-sink thrust chamber having a contraction ratio of 12 and a convergence half-angle of 45°. The expansion ratio was 8 with a 15° half-angle of divergence. The tests were performed with and without peripheral film cooling of the chamber wall near the injector. The cooling flows were varied from 2 to 7.5 percent of the hydrogen propellant weight flow.

With no peripheral film cooling, the average correlation coefficient C_d in the equation $St^* Pr^{*-.7} = C_d Re_d^{*-.2}$, where St, Pr, and Re_d are the Stanton, Prandtl, and Reynolds numbers, varied from a high of 0.056 near the injector to a low of 0.017 just downstream of the throat.

When the local diameter in the Reynolds number of the correlating equation was replaced by the axial distance from the injector, the correlation coefficient C_x varied from a high of 0.0346 near the injector to a low of 0.0214 upstream of the throat, a reduction of 66 percent in the overall axial variation of the correlation coefficient.

With peripheral film cooling, the average peak value of the correlation coefficient near the injector was reduced 50 percent with 7.5 percent film cooling over a range of chamber pressures of 426×10^4 to 584×10^4 newtons per square meter (618 to 847 psia). The average peak value of the correlation coefficient near the injector was reduced 25 percent for 2 and 3.75 percent film cooling over a range of chamber pressure of 105×10^4 to 286×10^4 newtons per square meter (153 to 415 psia).

The effects of peripheral film cooling dissipated before the convergence section of the thrust chamber.

INTRODUCTION

NERVA type nuclear rocket thrust chambers operate at heat-flux levels in excess of 32.7×10^6 watts per square meter (20 Btu/in.^{2}/sec) at the throat. For the stainless steel materials presently used in the thrust chamber design, heat-flux levels of this magnitude impose critical cooling problems for the rocket engine designer. To provide a reliable design for the long lifetimes required for the missions of interest, an accurate knowledge of both the coolant-side and hot-gas-side heat-transfer coefficients is essential.

Nuclear thrust chambers have geometric characteristics which differ from those of the chemical rocket thrust chamber: two such differences are contraction ratios of 12 to 20 necessitated by the large reactor core and contraction half-angles as high as 45°.

Since the geometric shape of the nuclear rocket thrust chamber may cause the heat-transfer characteristics to vary from those associated with the chemical rocket, an overall program was initiated at Lewis to study the heat-transfer characteristics of the nuclear rocket thrust chamber. This program includes experiments on both the coolant side and hot-gas side of rocket thrust chambers; however, the investigation reported herein is limited to the hot-gas side.

Several investigations have been conducted on the hot-gas side of rocket thrust chambers covering a wide range of geometries and configurations; however, most of these investigations were performed at heat flux levels below 1.6×10^6 watts per square meter (1 Btu/in.^{2}/sec) using heated air. References 1 to 5 give the results of some of these tests.

Reference 6 gives the results of a chemical rocket thrust chamber operating at heat fluxes in excess of 32.7×10^6 watts per square meter (20 Btu/in.^{2}/sec) at the throat using hydrogen oxygen as propellants, but the thrust chamber was restricted to a contraction ratio of 4.64 and a contraction half-angle of 30°.

Nuclear rocket thrust chambers have also been successfully fired in ground tests, but the instrumentation necessary to provide detailed heat-transfer data has been lacking.

Thus, to provide detailed hot-gas-side heat-transfer data pertinent to a nuclear rocket thrust chamber, the investigation reported herein was undertaken using a copper heat-sink thrust chamber having a 0.1092-meter- (4.3-in.-) diameter throat, a contraction ratio of 12, and a contraction half-angle of 45°. The expansion ratio was 8 with a 15° half-angle of divergence. The thrust chamber was instrumented with 36 calorimeters distributed circumferentially at 17 axial locations.

Since it is impractical to heat hydrogen to the temperature encountered in the nuclear chamber, gaseous hydrogen and liquid oxygen were chosen as propellants for this investigation. This propellant combination provided a practical and economical means of simulating the nuclear throat heat flux, and for the tests reported herein provided throat heat fluxes of up to 49×10^6 watts per square meter (30 Btu/in.^{2}/sec).

Preliminary tests conducted with steel heat-sink thrust chambers revealed a region of high heat transfer along the thrust chamber wall near the injector. It appeared that the high heat transfer was due to injector recirculation. In an effort to eliminate this hot spot region, the program was expanded to study the effect of peripheral film cooling on the heat transfer. To accomplish this, three injectors were modified to provide peripheral film cooling along the thrust chamber wall near the injector in amounts varying from 0 to 7.5 percent of the gaseous hydrogen propellant weight flow.

Whether or not recirculation of the type encountered in this program is inherent in a nuclear thrust chamber is not known; however, the film cooling results presented in this report should be applicable to other chemical rocket thrust chambers, and they may be applicable to a nuclear rocket thrust chamber. Since the effects of the film cooling disappear before the convergence section of the chamber, most of the data presented herein from the convergence section of the chamber to the thrust chamber exit should be applicable to the nuclear geometry.

The data are presented and compared by two correlating equations:

$$St^* Pr^{*\cdot 7} = C_d Re_d^{*-.2}$$

where the diameter is used in the Reynolds number as the characteristic dimension, and

$$St^* Pr^{*\cdot 7} = C_x Re_x^{*-.2}$$

where the axial distance from the injector face is used as the characteristic dimension in the Reynolds number. The relative effects of peripheral film cooling on the heat transfer near the injector are represented by comparison of the correlating coefficients C_d or C_x with those for no cooling.

The thrust chamber operated over a range of chamber pressures of 105×10^4 to 584×10^4 newtons per square meter (153 to 847 psia) and over an O/F range of 3.0 to 5.67 to provide a Reynolds number range over which to correlate the data.

SYMBOLS

A cross-sectional area, cm^2 ($in.^2$)

C correlation coefficient in equation $St^* Pr^{*\cdot 7} = CRe^{*-.2}$

c_p specific heat of material, J/(kg)(K) (Btu/(lb)($^\circ$R))

d nozzle diameter, cm (in.)

H enthalpy, J/kg (Btu/lb)

H_{aw}	adiabatic wall enthalpy, J/kg (Btu/lb)
h	heat-transfer coefficient, $W/(m^2)(K)$ $(Btu/(in.^2)(sec)(^oR))$
k	thermal conductivity of material, W/(m)(K) (Btu/(in.)(sec)(^{o}R))
L	rod length
O/F	oxidant-fuel ratio
P	pressure, N/m^2 (psi)
Pr^*	Prandtl number, $c_p^*\mu^*/k^*$
q	heat flow rate per unit area, W/m^2 $(Btu/in.^2/sec)$
Re_d^*	Reynolds number based on diameter, $\rho^* Vd/\mu^*$
Re_x^*	Reynolds number based on axial length, $\rho^* Vx/\mu^*$
S	entropy, J/(K) (Btu/(lb)(^{o}R))
St^*	Stanton number, $h/\rho^* Vc_p^*$
T	temperature, K (^{o}R)
T_{aw}	adiabatic wall temperature, $f(H_{aw}, P_s)$, K (^{o}R)
t	time, sec
$\dot{w}$	total weight flow rate, kg/sec (lb/sec)
x	axial distance from injector face at wall, cm (in.)
η_c	combustion efficiency
ρ	material density, kg/m^3 (lb/ft^3)
σ	standard deviation

Subscripts:

c	chamber or combustion condition
d	based on diameter
o	zero burning time
ref	reference
s	static
th	throat
theo	theoretical
tot	total
w	wall

X/L ratio of thermocouple distance from inner wall to total length of rod

x based on axial distance from injector face at wall

Superscript:

* reference enthalpy condition

APPARATUS AND TEST PROCEDURE

Thrust Chambers

A heavy wall, copper heat-sink thrust chamber was used to conduct the heat-transfer experiments. The thrust chamber contour and dimensions are shown in figure 1. The contraction and expansion area ratios were 12 and 8, respectively. Zirconia-coated mild

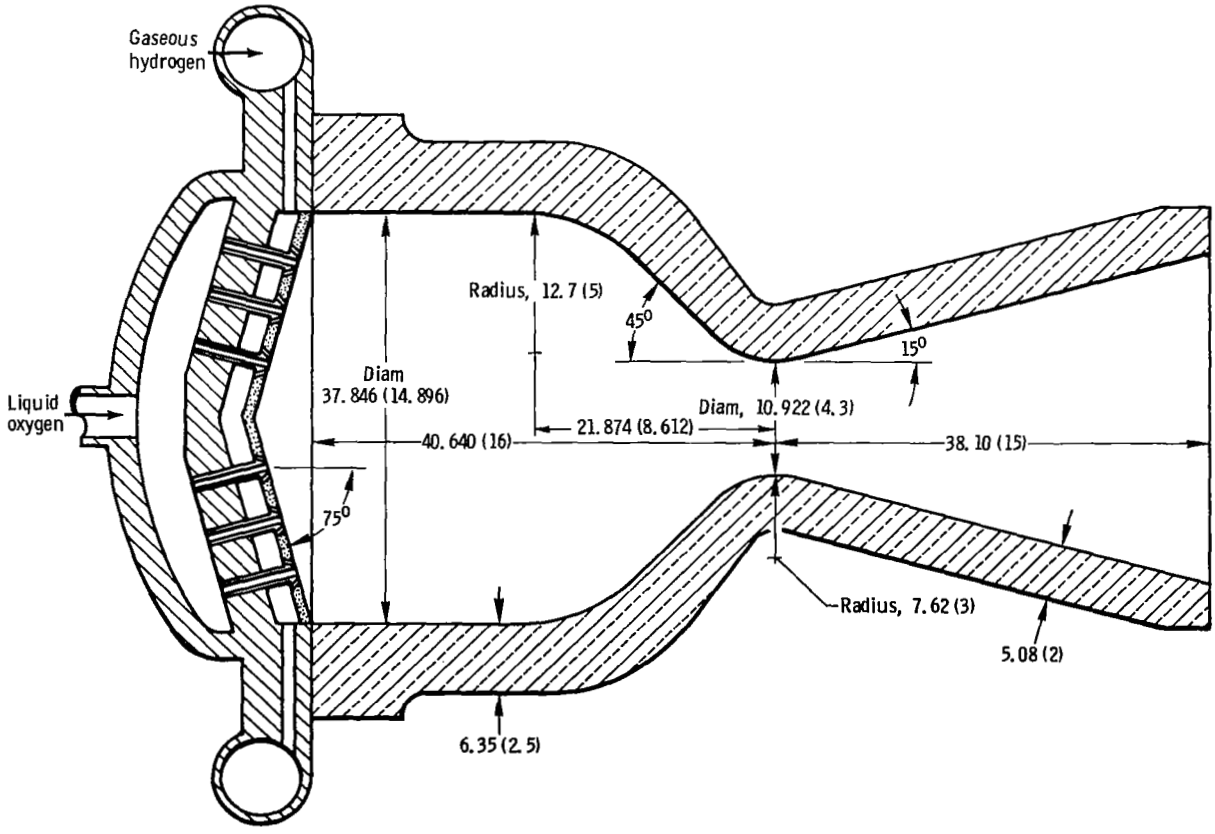

Figure 1. - Copper heat-sink rocket thrust chamber with coaxial, porous face injector. Area contraction ratio, 12:1; area expansion ratio, 8:1. Dimensions are in centimeters (in.).

steel thrust chambers of the same geometric contour were used for injector performance tests, developing the desired starting sequence, and facility checkout.

Injectors

Three 270-element, porous face coaxial injectors were fabricated for the investigation. The face plates were conically shaped as shown in figure 1. One injector was designed to operate over a chamber pressure range of 103×10^4 to 310×10^4 newtons per square meter (150 to 450 psia) and two injectors were designed to operate over a chamber pressure range of 345×10^4 to 586×10^4 newtons per square meter (500 to 850 psia). Figure 2 shows a typical injector.

To provide for peripheral film cooling along the thrust chamber wall, small holes were drilled through the porous face of the injector to allow a portion of the gaseous hydrogen propellant to be injected as a coolant. The holes were drilled at an angle such that the hydrogen jets would impinge on the chamber wall as shown in figure 3.

In order to compare the results of peripheral film cooling with those with no peripheral cooling during a single test, two injectors were divided into three 120° sectors. Each injector had two sectors with cooling and one sector with no cooling.

Figure 4 shows the configuration for each of the three injectors. The low chamber pressure injector (injector 1) provided peripheral film cooling flows of 0, 2.0, and 3.75

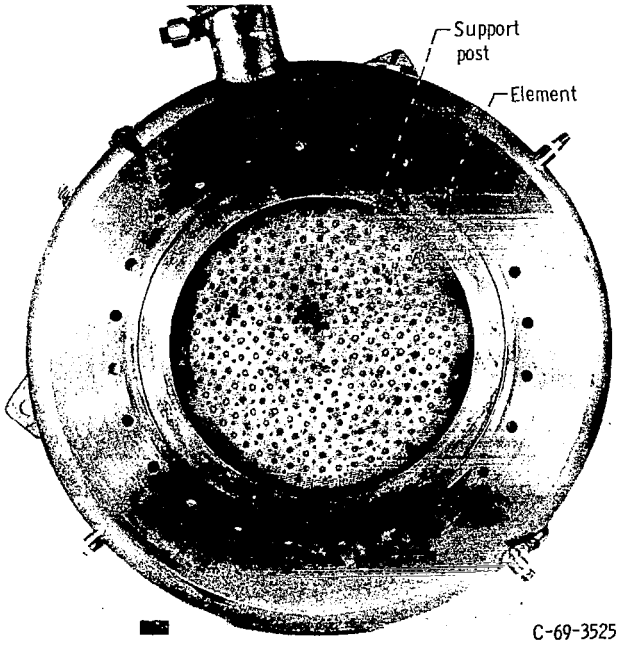

Figure 2. - High chamber pressure injector 2.

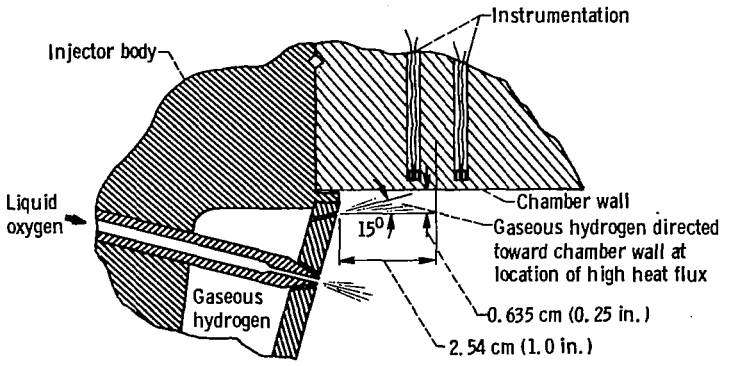

Figure 3. - Peripheral film cooling scheme.

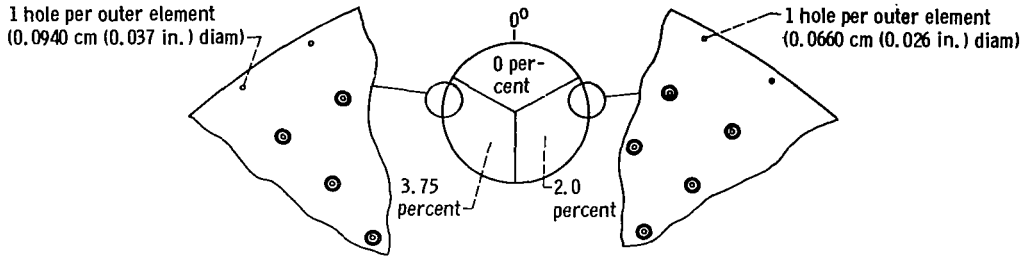

(a) Low chamber pressure range (injector 1).

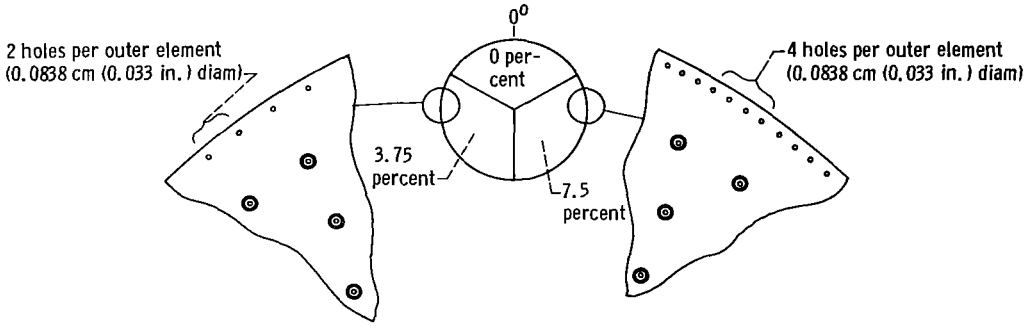

(b) High chamber pressure range (injector 2).

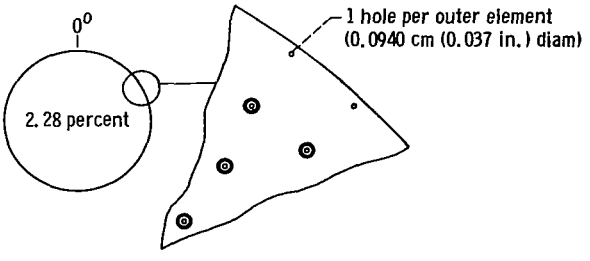

(c) High chamber pressure range (injector 3).

Figure 4. - Various injector configurations showing amount of peripheral cooling per sector and number of cooling holes per element in outer circle for film cooling flows of 0, 2, 2.28, 3.75, and 7.5 percent.

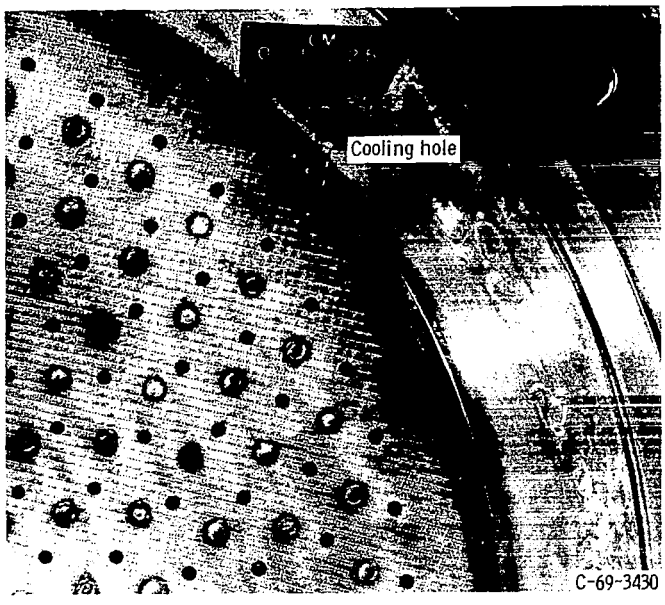

Figure 5. - Location of cooling holes in high chamber pressure injector 2. Chamber pressure, 345×10^4 to 586×10^4 newtons per square meter (500 to 850 psia); peripheral cooling, 7.5 percent.

percent. One high chamber pressure injector provided 0, 3.75, and 7.5 percent film cooling, while the other high chamber pressure injector provided 2.28 percent cooling around the entire outer periphery. The number of film cooling holes per outer row injector element also varied as shown in figure 4. Figure 5 shows the location of the holes for 7.5 percent peripheral cooling on high chamber pressure injector 2.

Copper Rod Calorimeter

Figure 6(a) shows the detail of the device used to measure heat flux. Oxygen free, high conductivity copper rods 7.62 centimeters (3.0 in.) and 0.5715 centimeter (0.225 in.) in diameter were instrumented with four 34 gage wire Chromel-Alumel thermocouples. The thermocouple balls were peened into small holes drilled into the surface of the rod. The rod length was chosen such that one-dimensional flow of heat in the rod approximated the radial flow of heat in the chamber wall, thus minimizing the temperature difference between the end of the rod and the adjacent wall. The rods were threaded at one end for installation into the chamber wall. The thread was cut such that the major diameter of the thread was larger than the diameter of the unthreaded portion of the rod. This was done so that the average cross-sectional area of the threaded portion of the rod equaled the cross-sectional area of the unthreaded portion of the rod. Before installation, the

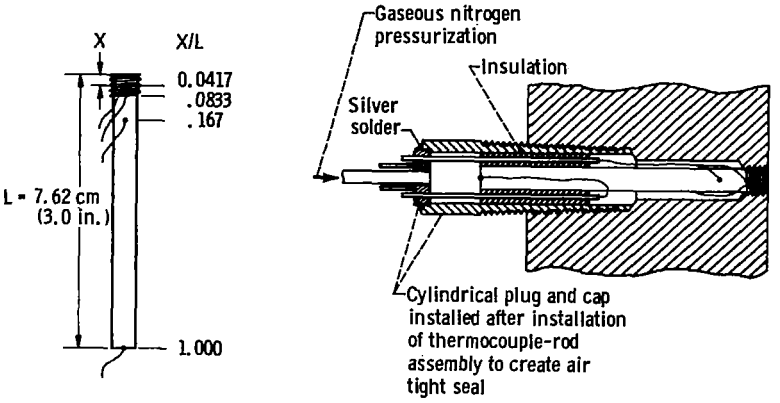

(a) Copper rod showing thermocouple locations.

(b) Installation of rod assembly.

Figure 6. - Copper rod calorimeter.

threaded portion of the rod was oxidized to minimize the flow of heat from the rod to the adjacent wall.

The thermocouple rod assembly was then installed into the chamber wall as shown in figure 6(b). Experience has shown that after several thermal cycles the threaded area of the rod loosens sufficiently so that hot-gas leaks into the cavity surrounding the rod. Therefore, the back side of the rod cavity was sealed to prevent continuous leakage of hot gas through the cavity. Further provision was made to allow pressurization of the rod cavity to minimize the leakage into the cavity. Care was taken to insure that the pressure in the cavity was set to a value lower than the wall static pressure encountered during a given test so that inadvertent film cooling of the rod did not occur. The pressure in the cavity was set to 95 percent of the expected static wall pressure.

In order to measure the heat flux near the injector in sufficient detail to evaluate the effects of film cooling, several calorimeters were required; however, the copper rod calorimeter, due to its bulky size interfered with the injector manifold and could not be used. Thus, a one thermocouple calorimeter was devised for use near the injector.

One Thermocouple Calorimeter

Figure 7(a) shows the detail of the one thermocouple calorimeter. The assembly consisted of 0.0508-centimeter (0.020-in.) Chromel-Alumel thermcouple wires inserted in a 0.3175-centimeter (0.125-in.) diameter copper tube, which is 0.3175 centimeter (0.125 in.) in height. The tube was then filled with silver solder.

Figure 7(b) shows the installation of the calorimeter in the thrust chamber wall. A 0.3175-centimeter (0.125-in.) diameter hole was end milled to a depth of 0.254 centi-

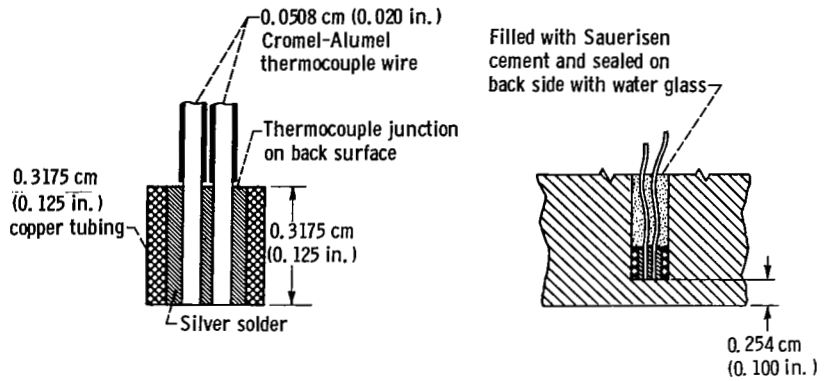

(a) Thermocouple calorimeter detail. (b) Installation of calorimeter in chamber wall.

Figure 7. - One thermocouple calorimeter.

meter (0.100 in.) from the inner wall. The thermocouple assembly was then peened into the hole to insure intimate contact with the surrounding surfaces. To prevent moisture from entering the hole, the hole was filled with Sauerisen cement and sealed on the back side with water glass.

Of the two methods used in these tests to measure heat flux, the copper rod calorimeter was the preferred instrument. Since each thermocouple on the rod allowed an independent calculation of the heat-transfer coefficient and the gas wall temperature, comparisons could be made to determine which data appeared to be questionable because of bad thermocouple readings. Although the single thermocouple calorimeter was not considered to be the best instrument for heat flux measurement, it was considered to be sufficiently accurate to reveal the relative effects of the peripheral film cooling.

Instrument Locations

Fifteen pressure taps were installed along the thrust chamber wall to measure the local static pressure. Figure 8 shows the axial and circumferential location of the pressure taps, copper rod calorimeters, and the single thermocouple calorimeters. It should be noted that stations 5 and 6 are the same axial location. This nomenclature was adopted to distinguish between the two types of calorimeters installed at this axial location. Station 5 designates the location of the single thermocouple calorimeters, while station 6 designates the location of the copper rod calorimeters. Figure 9 shows the fully instrumented copper-heat-sink thrust chamber installed in the test facility.

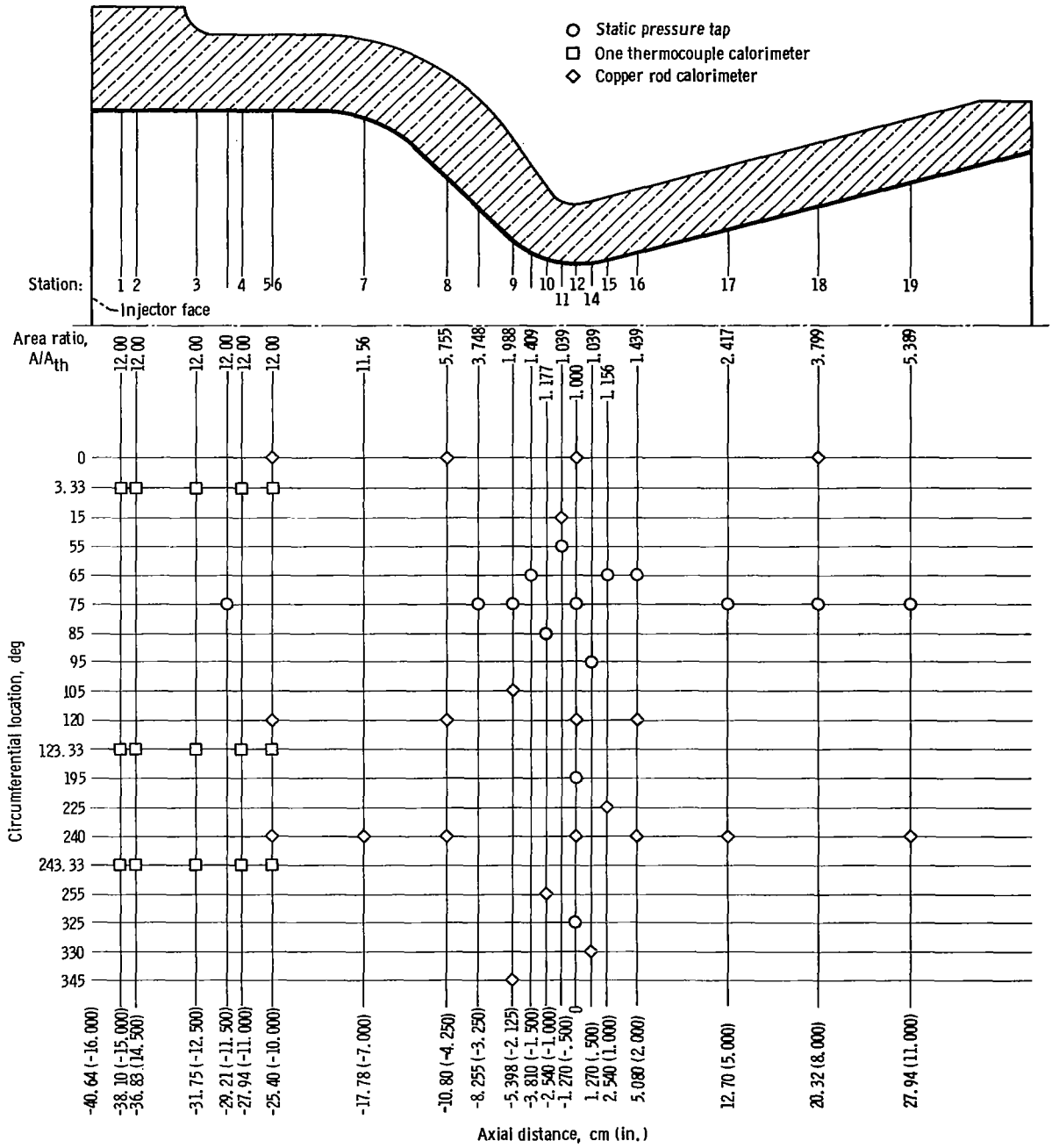

Figure 8. - Instrumentation locations. Angular position as viewed from thrust chamber exit.

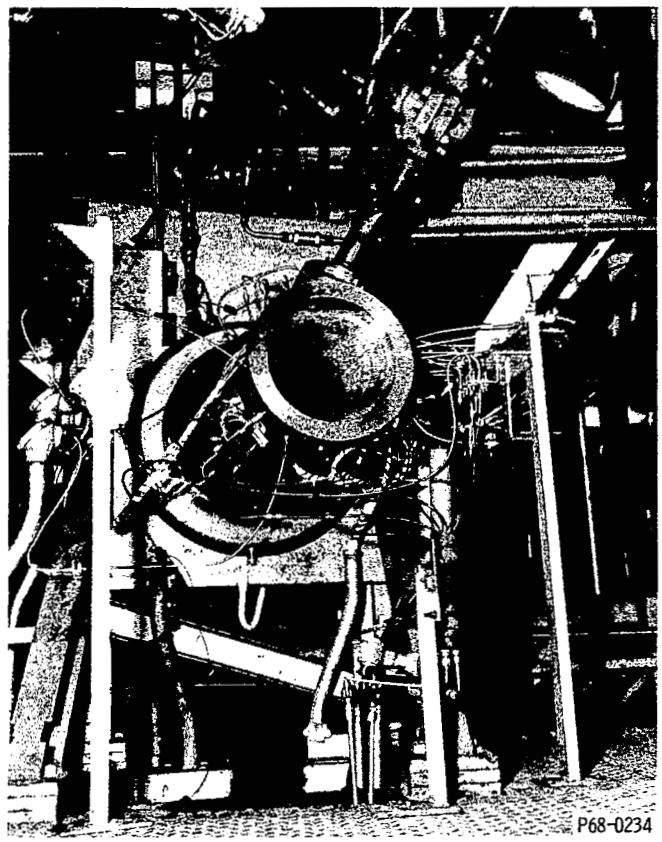

Figure 9. - Copper heat-sink thrust chamber installed in test facility.

Test Procedure

Gaseous hydrogen and liquid oxygen were supplied by pressurized tanks. The propellant valves were scheduled to open to a preset position in order to reach the desired chamber pressure in the shortest possible time. After the preset conditions were achieved, the O/F and P_c controllers were turned on to maintain the desired operating condition. Using this method, full chamber pressure could be achieved in 0.02 to 0.06 second. This approximated a step function in T_{aw} which allowed a simpler solution to be used for computing h.

Data Recording

All the data, including the propellant weight flow parameters, chamber pressure, static pressure measurements, and the thermocouple readings, were recorded on a high

speed digitizer having a basic sampling rate of 31 250 words per second. The data parameters were recorded in a 125-word block which provided a 0.004-second cycle time between samples of a given parameter. Chamber pressure was recorded six times in the data block to reduce the time between samples. This was done so that chamber pressure could be used to establish time zero for the start of computing the heat-transfer parameters. The data were smoothed over 25 blocks which eliminated 60 hertz noise and minimized the effects of random noise. After smoothing, all data parameters were picked at a common time for computing.

CALCULATION PROCEDURE

Constant Heat-Transfer Coefficient Method

The heat-transfer coefficient h was determined from the solution of the transient conduction equation for a semi-infinite slab. The equation appears in closed form in reference 7. When substitution of the dimensionless variables is made into the equation of reference 7, the equation appears in the form

$$\varphi = \frac{T_{X/L} - T_o}{T_{aw} - T_o} = \operatorname{erfc} \frac{\frac{hX}{k}}{2\sqrt{\frac{h^2 t}{k\rho c}}} - \exp\left(\frac{hX}{k} + \frac{h^2 t}{k\rho c}\right) \operatorname{erfc}\left(\frac{\frac{hX}{k}}{2\sqrt{\frac{h^2 t}{k\rho c}}} + \sqrt{\frac{h^2 t}{k\rho c}}\right) \tag{1}$$

where

$$\operatorname{erfc}(z) = 1 - \frac{2}{\sqrt{\pi}} \int_0^{(z)} e^{-z^2}\, dz$$

t is the time, T_o the initial temperature at $t = 0$, $T_{(X/L)}$ the temperature at a given thermocouple location on the rod at time t, and T_{aw} the adiabatic wall temperature.

The conductivity k, density ρ, and specific heat c are the material properties, and they were inserted into equation (1) at a reference temperature as suggested in reference 8. For conduction in simple metals,

$$T_{ref} = \frac{T_{(X/L)=0} - T_o}{4} + T_o$$

where $T_{(X/L)=0}$ is the temperature at the wall at time t.

When a given time t is picked for computing, all of the properties in equation (1) can be evaluated from the known value of $T_{X/L}$ at time t and the known value of T_o. The heat-transfer coefficient h is then determined by an iteration scheme whereby values of h are guessed until the right side of equation (1) equals the left side. However, to evaluate the left side of the equation T_{aw} must be known:

$$T_{aw} = T_s + \sqrt[3]{Pr^*}\,(T_c - T_s)$$

The determination of T_c, T_s, and the transport properties is discussed in the Combustion Temperature and Thermodynamic and Transport Property sections. A more detailed description of the boundary conditions and limitations which apply to equation (1) is given in reference 6.

It should be noted that heat flux q is the quantity really measured by the calorimeter, and not h or T_{aw}. Therefore, in the case of film cooling a problem arises in determining the T_{aw} to be used in equation (1). Since h and T_{aw} are tied together and T_{aw} was not measured, T_{aw} is assumed to be that for the injector O/F, with no film cooling, and h is calculated accordingly. However, the effectiveness of the film cooling can be evaluated by comparing the heat transfer with film cooling with that for no film cooling.

Combustion Temperature

The combustion temperature T_c is a function of chamber pressure P_c, oxygen/fuel ratio O/F, and combustion efficiency η_c. With the enthalpy of the incoming propellants, the measured P_c, and O/F, theoretical values of T_c and $\dot{w}/A_{th}$ can be computed which give Mach 1 at the throat of the thrust chamber. When the measured weight flow is greater than the theoretical weight flow, a new T_c can be calculated which will allow the measured weight flow to pass through the throat at Mach 1. In this case Mach 1 is for one-dimensional flow. This new combustion temperature is considered to be the measured combustion temperature $T_{c,meas}$. Combustion efficiency is then defined as

$$\eta_c = \frac{T_{c,meas}}{T_{c,theo}}$$

For the data reported herein, the measured weight flows resulted in a calculated combustion efficiency of 100 percent, so $T_{c,meas}$ was assumed to be $T_{c,theo}$.

Thermodynamic and Transport Properties

Thermodynamic and transport properties are required at each measuring station in the thrust chamber to determine the local heat-transfer coefficient and for use in the correlating equations. The transport properties were evaluated at Eckert's reference enthalpy (ref. 9) and the local static pressure. When $\sqrt[3]{Pr}$, the recovery factor for turbulent flow, is inserted in the reference enthalpy equation of reference 9, the equation reduces to

$$H^* = H_s + 0.5\,(H_w - H_s) + 0.22\,\sqrt[3]{Pr^*}\,(H_c - H_s)$$

The theoretical one-dimensional static pressure was used for axial stations 1 to 8. The measured pressure was used for axial stations 9 to 19, where the experimental static pressure deviated from the theoretical pressure. Figure 10 shows a comparison of the theoretical and experimental pressure ratios for a typical test run.

The thermodynamic and transport properties are assumed to be those for equilibrium composition and are calculated in the same manner as in reference 6.

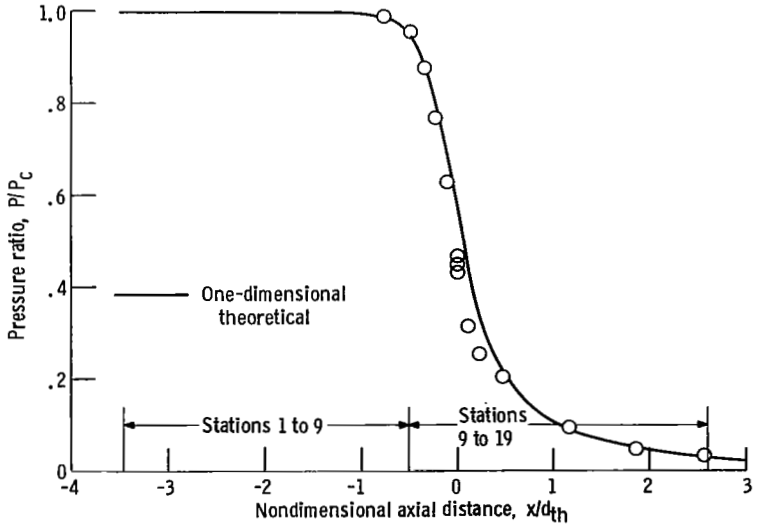

Figure 10. - Wall pressure ratio profile. Chamber pressure, $P_c = 211 \times 10^4$ newtons per square meter (306 psia); oxidant-fuel ratio, O/F = 5.33.

Correlating Equations

Two nondimensional correlating equations are used to present the data. Both equations are groupings of Stanton, Prandtl, and Reynolds numbers and appear in the forms

$$St^* Pr^{*.7} = C_d Re_d^{*-.2} \tag{2}$$

and

$$St^* Pr^{*.7} = C_x Re_x^{*-.2} \tag{3}$$

The difference between the two equations is the characteristic dimension used in the Reynolds number. In equation (2) the local diameter is used and in equation (3) the axial distance from the injector is used. The superscript stars indicate that all transport properties were evaluated at reference enthalpy H^* and local static pressure P_s.

RESULTS AND DISCUSSION

Fourteen test runs were made over a range of O/F's and chamber pressures. Five tests were run in the low P_c range with injector 1, four tests were run in the high P_c range with injector 2, and five tests were run in the high P_c range with injector 3. Table I gives a summary of the run conditions and peripheral film cooling configurations. The missing run numbers in the table represent those calibration runs and aborted runs where no data were taken.

Figures 11(a) to (r) show the data in nondimensional form where the Stanton-Prandtl grouping of the data is plotted as a function of Reynolds number. A line appears in each figure where

$$St^* Pr^{*.7} = 0.026\ Re_d^{*-.2}$$

The value of 0.026 represents the correlating coefficient for convective heat transfer from a fluid to a pipe wall under fully developed turbulent flow conditions (ref. 9). Early correlating schemes for rocket thrust chamber heat transfer used the 0.026 value in the correlating equation for determining the hot-gas-side heat-transfer coefficients throughout the entire thrust chamber (ref. 10). It was subsequently determined that the correlating coefficient was not constant, but in fact deviated from 0.026 in a plus and minus direction depending on the location in the thrust chamber. However, the line appears in

TABLE I. - RUN CONDITIONS

Run	Chamber pressure		Oxidant-fuel ratio, O/F	Peripheral cooling, percent		
	N/m^2	psia				
Low chamber pressure injector 1						
11	211.0×10^4	306	5.33	0	2.0	3.75
12	211.0	306	4.01	↓	↓	↓
15	210.3	305	3.11			
18	286.1	415	5.44			
25	105.5	153	5.50			
High chamber pressure injector 3						
28	364.0×10^4	528	5.00	2.28	2.28	2.28
31	488.8	709	5.80	↓	↓	↓
34	486.8	706	4.86			
37	428.2	621	3.08			
43	570.9	828	4.88			
High chamber pressure injector 2						
47	433.0×10^4	628	3.75	0	3.75	7.50
48	433.7	629	3.43	↓	↓	↓
51	426.1	618	5.23			
54	584.0	847	5.28			

figure 11 so that a comparison can be made of the data relative to that for fully developed turbulent pipe flow.

Film Cooling

The data for peripheral film cooling and those for no cooling are shown for stations 1 to 7 in figures 11(a) to (g). A line having a -.2 slope and representing a least squares fit of the no cooling data is shown on each figure. The correlating equation representing that line is also shown. Furthermore, a dashed line was drawn through each set of film cooling data to aid the reader in identifying the relative effect of various amounts of film cooling on the heat-transfer level. It is readily apparent that a slope other than -.2 would best fit the film cooling data, although this appears to be true for the no cooling data as well for stations 1 to 6. However, the -.2 slope has been maintained for correlating the no film cooling data since the range of Reynolds numbers is insufficient to justify a change from the turbulent flow model.

Run	Chamber pressure, P_c		Oxidant-fuel ratio, O/F	Cooling, percent				
	N/M^2	psia		0	2.0	2.28	3.75	7.5
11	211.0×10^4	306	5.33	○	◐		◑	
12	211.0	306	4.01	□	◧		◨	
15	210.3	305	3.11	◇	◆		◆	
18	286.1	415	5.44	▽	▼		▼	
25	105.5	153	5.50	◁	◀		◀	
28	364.0	528	5.00			◧		
31	488.8	709	5.80			◧		
34	486.8	706	4.86			◆		
37	428.2	621	3.08			◆		
43	570.9	828	4.88			◧		
47	433.0	628	3.75	△			△	▲
48	433.7	629	3.43	◺			◣	◣
51	426.1	618	5.23	◺			◨	◨
54	584.0	847	5.28	◺			◨	◨

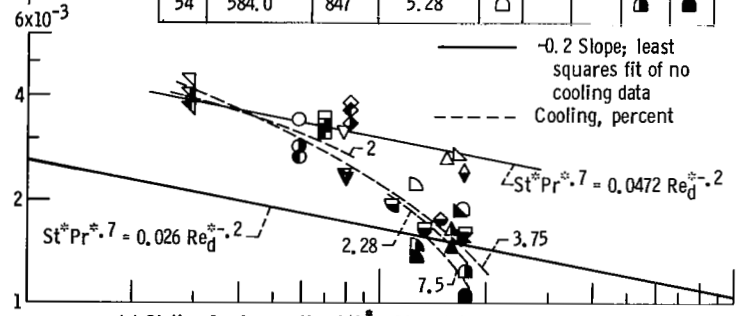

(a) Station 1. Area ratio, $A/A^* = 12$; axial distance from throat, x = -38.1 centimeters (-15 in.).

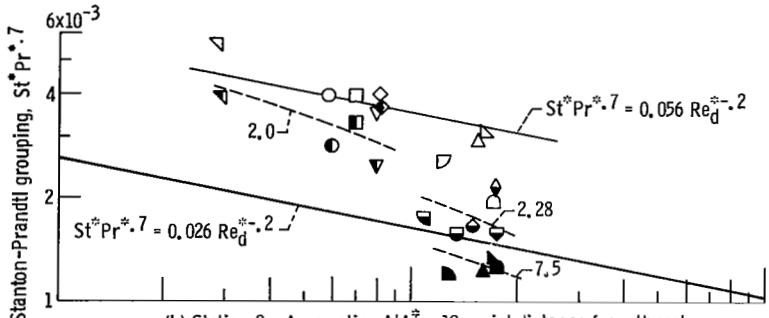

(b) Station 2. Area ratio, $A/A^* = 12$; axial distance from throat, x = -36.8 centimeters (-14.5 in.).

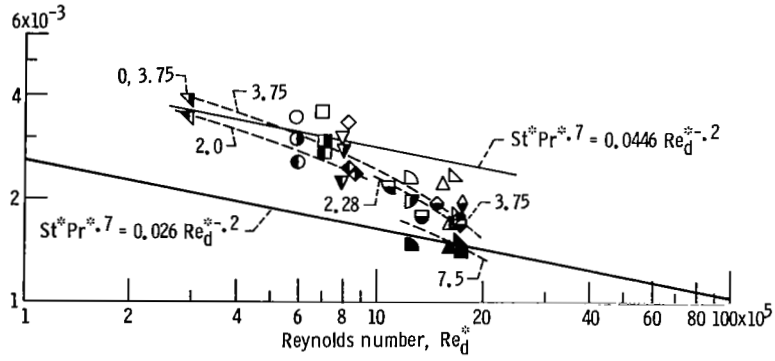

(c) Station 3. Area ratio, $A/A^* = 12$; axial distance from throat, x = -31.75 centimeters (-12.5 in.).

Figure 11. - Stanton-Prandtl grouping as function of Reynolds number. Open symbols on parts (h) to (r) represent average of all data at given axial location.

Run	Chamber pressure, P_c		Oxidant-fuel ratio, O/F	Cooling, percent				
	N/M^2	psia		0	2.0	2.28	3.75	7.5
11	211.0×10^4	306	5.33	○	◐		◑	
12	211.0	306	4.01	□	◧		◨	
15	210.3	305	3.11	◇	◆		◆	
18	286.1	415	5.44	▽	▼		▼	
25	105.5	153	5.50	◁	◀		◀	
28	364.0	528	5.00			◧		
31	488.8	709	5.80			◧		
34	486.8	706	4.86			◆		
37	428.2	621	3.08			◆		
43	570.9	828	4.88			◧		
47	433.0	628	3.75	△			▲	▲
48	433.7	629	3.43	◺			◣	◣
51	426.1	618	5.23	◻			◧	◧
54	584.0	847	5.28	◻			◧	●

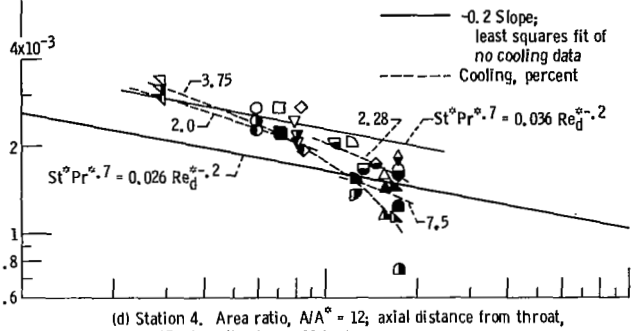

(d) Station 4. Area ratio, $A/A^* = 12$; axial distance from throat, x = -27.94 centimeters (-11 in.).

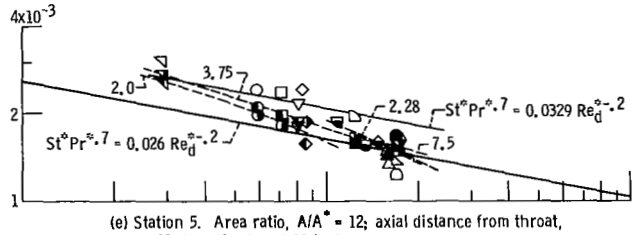

(e) Station 5. Area ratio, $A/A^* = 12$; axial distance from throat, x = -25.4 centimeters (-10 in.).

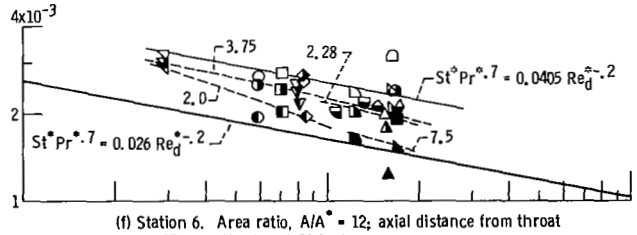

(f) Station 6. Area ratio, $A/A^* = 12$; axial distance from throat x = -25.4 centimeters (-10 in.).

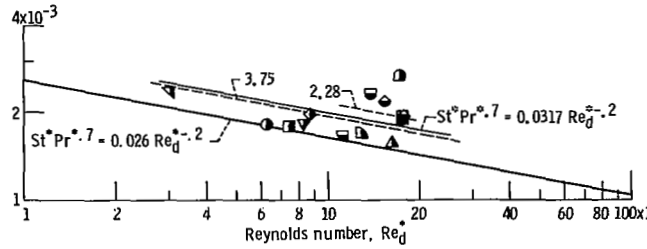

(g) Station 7. Area ratio, $A/A^* = 11.156$; axial distance from throat, x = -17.78 centimeters (-7 in.).

Stanton-Prandtl grouping, $St^*Pr^{*.7}$

Figure 11. - Continued.

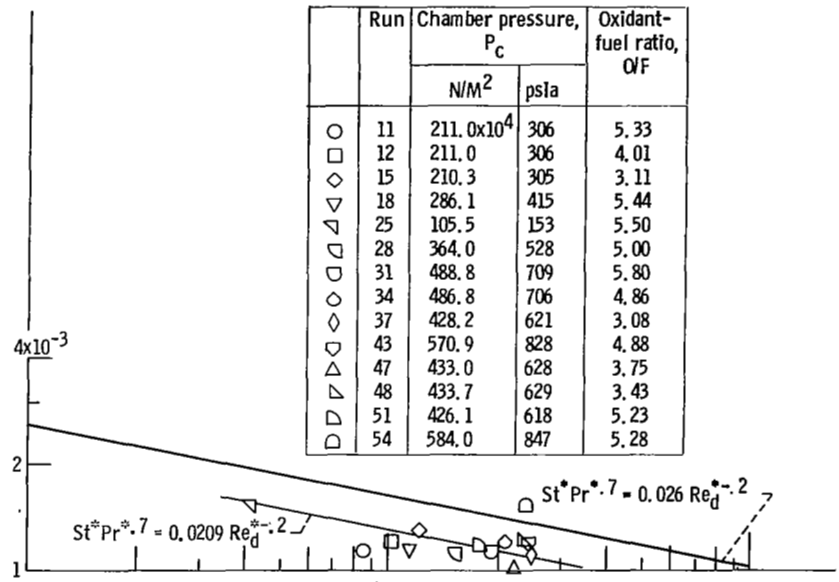

(h) Station 8. Area ratio, $A/A^* = 5.755$; axial distance from throat, $x = -10.795$ centimeters (-4.25 in.).

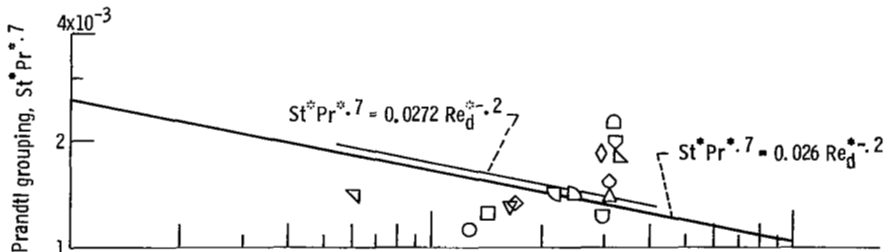

(i) Station 9. Area ratio, $A/A^* = 1.988$; axial distance from throat, $x = -5.398$ centimeters (-2.125 in.).

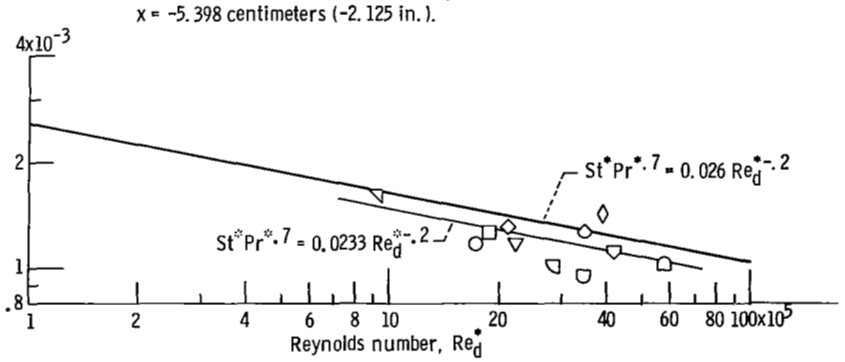

(j) Station 10. Area ratio, $A/A^* = 1.777$; axial distance from throat, $x = -2.54$ centimeters (-1 in.).

Figure 11. - Continued.

	Run	Chamber pressure, P_c		Oxidant-fuel ratio, O/F
		N/m^2	psia	
○	11	211.0×10^4	306	5.33
□	12	211.0	306	4.01
◇	15	210.3	305	3.11
▽	18	286.1	415	5.44
◁	25	105.5	153	5.50
◁	28	364.0	528	5.00
▢	31	488.8	709	5.80
◇	34	486.8	706	4.86
◇	37	428.2	621	3.08
▽	43	570.9	828	4.88
△	47	433.0	628	3.75
▷	48	433.7	629	3.43
▷	51	426.1	618	5.23
▢	54	584.0	847	5.28

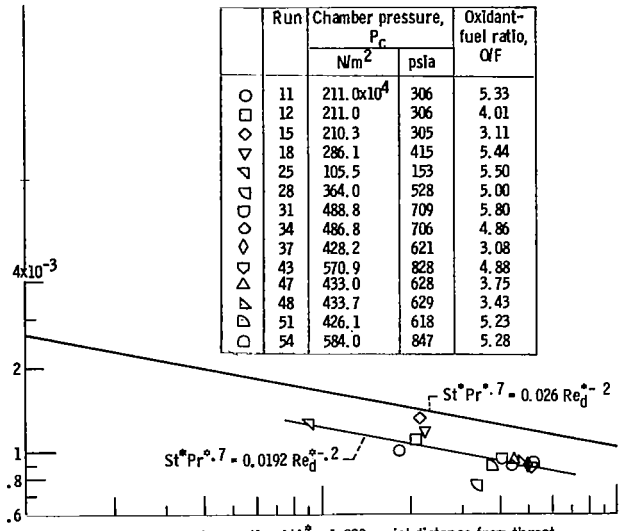

(k) Station 11. Area ratio, $A/A^* = 1.039$; axial distance from throat, x = -1.270 centimeters (-0.5 in.).

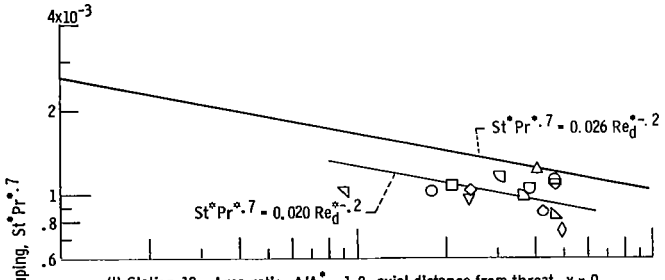

(l) Station 12. Area ratio, $A/A^* = 1.0$; axial distance from throat, x = 0.

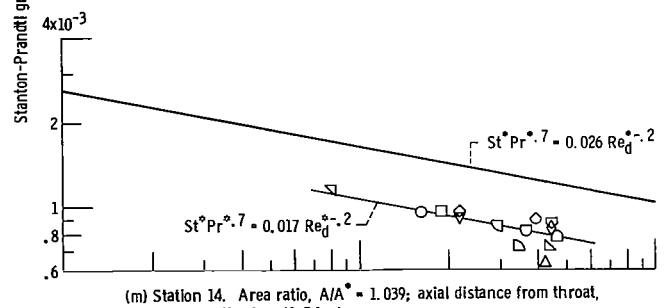

(m) Station 14. Area ratio, $A/A^* = 1.039$; axial distance from throat, x = 1.27 centimeters (0.5 in.).

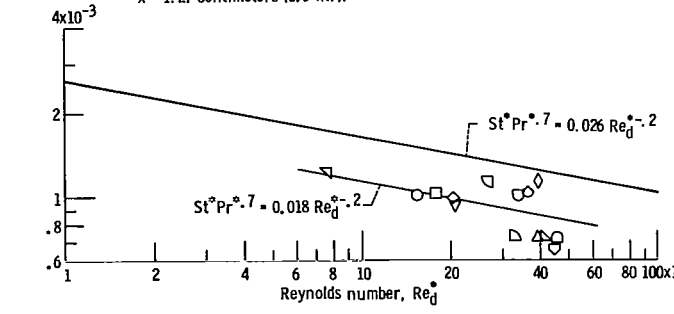

(n) Station 15. Area ratio, $A/A^* = 1.156$; axial distance from throat, x = 2.54 centimeters (1 in.).

Figure 11. - Continued.

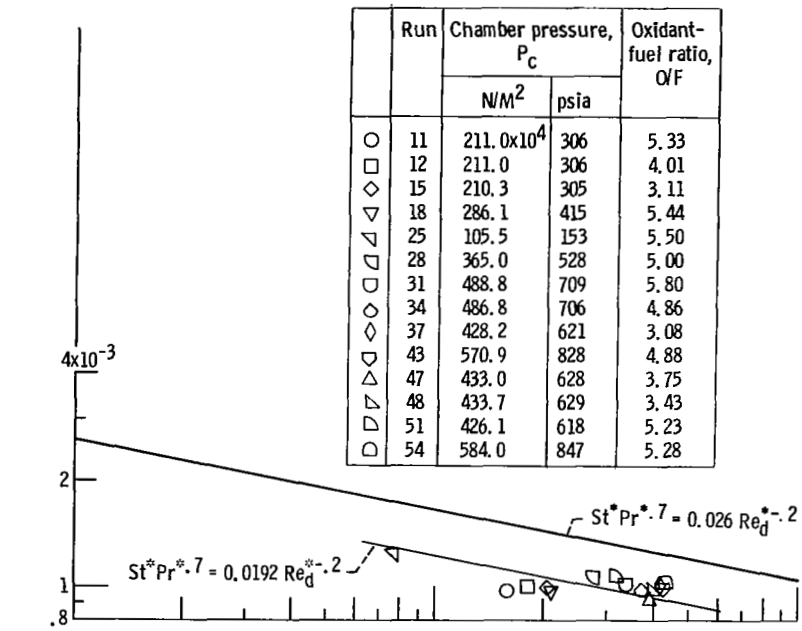

(o) Station 16. Area ratio, $A/A^* = 1.439$; axial distance from throat, x = 5.08 centimeters (2 in.).

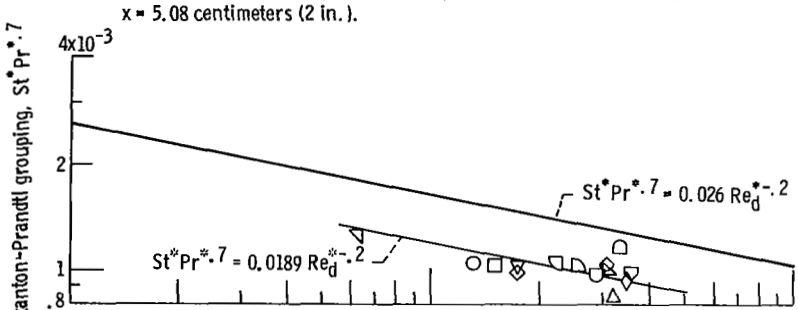

(p) Station 17. Area ratio, $A/A^* = 2.417$; axial distance from throat, x = 12.70 centimeters (5 in.).

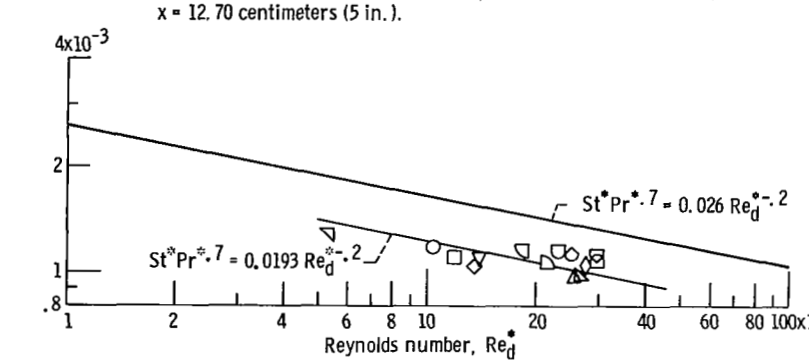

(q) Station 18. Area ratio, $A/A^* = 3.799$; axial distance from throat, x = 20.32 centimeters (8 in.).

Figure 11. - Continued.

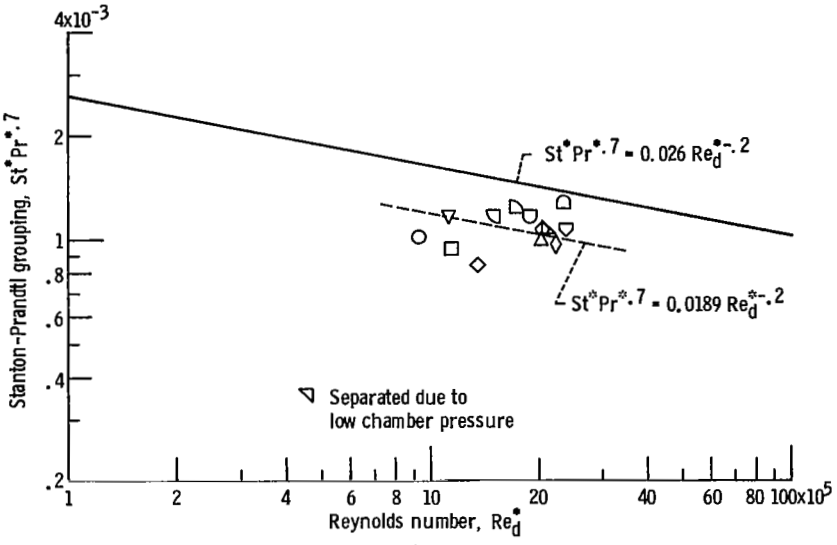

(r) Station 19. Area ratio, $A/A^* = 5.389$; axial distance from throat, x = 27.94 centimeters (11 in.).

Figure 11. - Concluded.

The reduction in heat transfer is about equal for the 2.0, 2.28, and 3.75 percent cooling data, with the 2.0 and 2.28 percent data falling below the 3.75 percent data at some stations. For the most part, the data for 7.5 percent cooling shows the largest reduction in heat transfer, although some of the 3.75 percent data fall below the 7.5 percent data at station 4 (fig. 11(d)). It can be seen that the film cooling is most effective at station 2 (fig. 11(b)) which was expected since the cooling streams were made to impinge on the wall at this location. Station 2 was also the location of maximum heat transfer in the chamber for no cooling.

Inspection of the data for station 5 (fig. 11(e)) shows that the effects of film cooling have diminished as evidenced by the fact that the data for film cooling have nearly converged with the data for no film cooling. This is especially evident at the higher Reynolds numbers. At station 6 (fig. 11(f)), which is at the same axial location as station 5, the data are considerable more scattered and the convergence of the film cooling data with the no cooling data is not as well defined. The overall level of heat transfer is also higher at station 6 as evidenced by the correlating coefficient which equals 0.0405 at station 6 and 0.0329 at station 5. There are two possible explanations for the discrepancy between the station 5 and station 6 data. First, the calorimeter at station 5 is the single thermocouple instrument, whereas the calorimeter at station 6 is the first in the axial array of the copper rod calorimeters; however, it is believed that a discrepancy in the data of this magnitude is not entirely due to the difference in instrumentation. The other explanation is that the instrumentation at stations 5 and 6 is not in the same circumferential

location (see fig. 8). In this case, the instruments at station 6 are in line with the injector elements in the outer row, whereas the instruments at station 5 are located between the elements in the outer row. Thus, it is likely that O/F zoning between the injector elements affected the heat transfer near the injector, and that the discrepancy in the data at stations 5 and 6 was caused by the injector rather than a result of the type of instrumentation used to take the data.

Normally, one thinks of film cooling reducing the heat flux to the wall by lowering the adiabatic wall temperature, and the more film cooling that is injected, the lower the heat flux should be. However, in the case where hydrogen is used as the film cooling media, it is possible that the reduction of the heat flux at one location could lead to an increase in heat flux at another location, even though the adiabatic wall temperature of the film is lower than that of the core. This could occur because the heat-transfer coefficient for pure hydrogen is considerably higher than that of a hydrogen-oxygen combination at an O/F of 5.5. Thus, even though the hydrogen film is reducing the heat flux to the wall at one location because of its low adiabatic wall temperature, the hydrogen film could be heated sufficiently by the core at some other location such that the combined effect of the high hydrogen heat-transfer coefficient and the resulting adiabatic wall temperature could create a heat flux higher than that encountered with no film cooling. This also might account for what appears to be inconsistencies in some of the cooling data.

Results for Nozzle Section Where Film Cooling is no Longer Effective

Figure 11(g) shows the data for station 7. Since there was only one calorimeter at this station, data exist for only two conditions, 2.28 and 3.75 percent cooling. Thus, no direct comparison with a no film cooling condition can be made. Although the data for the two cooling conditions are shown separately rather than averaged together, the correlating line represents the least squares fit of all of the data and is assumed to be representative of a no cooling condition. A comparison of the film cooling data with those of no film cooling for stations 8 to 19 revealed that the effects of film cooling had dissipated and could not be distinguished from those data with no film cooling within the spread of the data. Therefore, the data from all of the calorimeters at a given station were averaged together and shown as a single point for each run condition. These data are shown in figures 11(h) to (r). A line representing the least squares fit of the data is also shown. The -.2 slope has been maintained in all cases, and for the most part, the data are well represented by a line having this slope.

The data at station 9 (fig. 11(i)) do not lie along a line with a -.2 slope. In fact, in the high Reynolds number range, the slope approaches infinity. No explanation is available to describe the behavior of the data. However, inspection of the data from each of

the two calorimeters at station 9 reveals that the data agree within plus and minus 4 percent about the average for all the runs, with a maximum spread of plus and minus 10 percent for run 48. Thus, the behavior of the data cannot be attributed to instrumentation errors.

Correlation Coefficient C_d

To better portray the local level of heat transfer in the thrust chamber relative to that for fully developed turbulent pipe flow (i.e., $C_d = 0.026$), the local correlation coefficient C_d in the Stanton-Prandtl grouping is shown as a function of axial distance in figure 12. Each point represents the correlation coefficient obtained from a least squares fit of the data shown in figure 11. Due to the different pressure ranges and cooling flows associated with each injector, the results shown in figure 12 have been separated according to the injector used and amount of film cooling. Since stations 5 and 6 are the same location, but have different values of C_d, a dashed line has been connected between the average value of C_d in each sector at stations 5 and 6 with the value of C_d at station 7. A dashed line has also been drawn between the C_d's of stations 1 and 3 for 3.75 percent film cooling since the calorimeter was lost at station 2 in the 3.75 percent sector and no data exist for that location.

The results for the low P_c injector appear in figure 12(a). With no film cooling, the value of C_d near the injector is about 2.5 times greater than that for the fully developed turbulent pipe flow. When film cooling is injected, the reduction in C_d is about equal for 2.0 and 3.75 percent film cooling, with the 2.0 percent cooling somewhat more effective than the 3.75 percent cooling. The maximum reduction in C_d is 23 percent at station 2 with 2.0 percent cooling. However, the level of C_d at station 2 is still 80 percent above the 0.026 value. From stations 8 to 19 all the C_d's are below the 0.026 line with the average value about 27 percent lower than 0.026.

The values of C_d for the high P_c injector 2 are shown in figure 12(b). Inspection of figures 12(a) and (b) shows that the no cooling C_d's for the high P_c range lie, for the most part, below the C_d's with film cooling of the low P_c injector, with the peak value of C_d 27 percent lower at station 2. When film cooling was injected, the values of C_d were reduced to a range of 0.020 to 0.030. The peak value of C_d at station 2 was reduced 50 percent with 7.5 percent film cooling. As was the case for the low P_c injector, the values of C_d remain below the 0.026 line from station 8 to 19 with the exception of the large spike in C_d at station 9.

Figure 12(c) shows the C_d's for high P_c injector 3, which provided 2.28 percent film cooling around its entire periphery. Therefore, direct comparison of the film cooling C_d's with those with no film cooling cannot be made. However, inspection of fig-

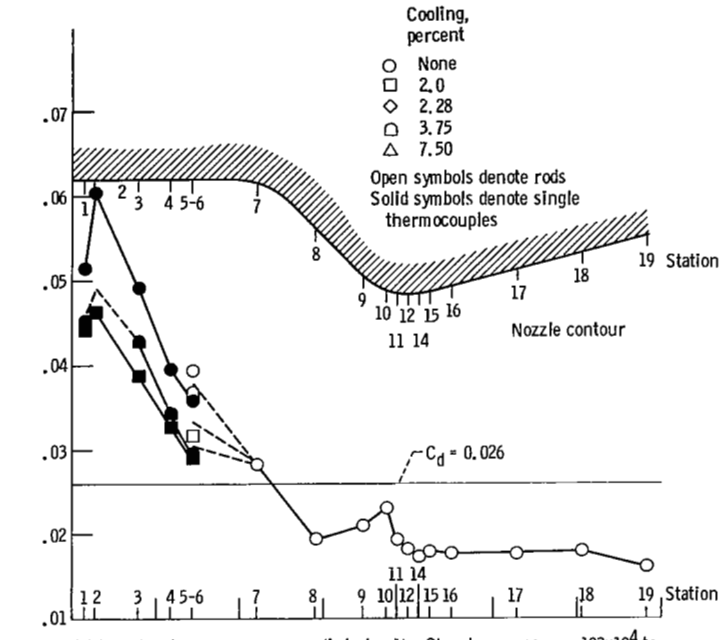

(a) Low chamber pressure range (injector 1). Chamber pressure, 103×10^4 to 286×10^4 newtons per square meter (150 to 415 psia).

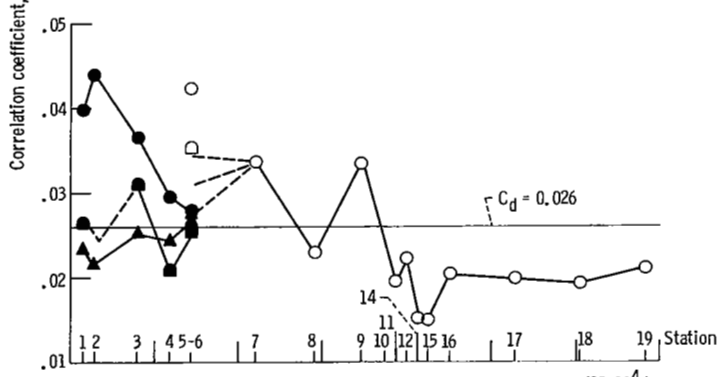

(b) High chamber pressure range (injector 2). Chamber pressure, 425×10^4 to 583×10^4 newtons per square meter (617 to 846 psia).

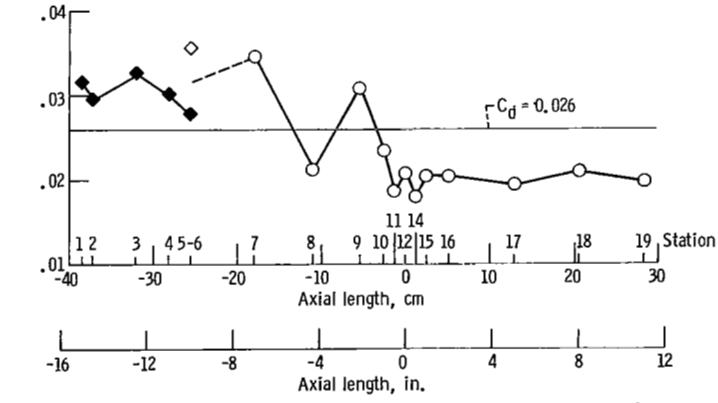

(c) High chamber pressure range (injector 3). Chamber pressure, 364×10^4 to 571×10^4 newtons per square meter (528 to 828 psia).

Figure 12. - Correlation coefficient C_d as function of axial length for $St^* Pr^{*.7} = C_d Re_d^{*-.2}$.

ures 12(b) and (c) show that the C_d's for stations 1 to 6 of high P_c injector 3 lie just above those for 3.75 percent cooling of high P_c injector 2. Thus, the data from the two high P_c injectors appear quite comparable.

It can be seen that the level of heat transfer near the injector appears to be a function of the P_c range, as the values of C_d for the low P_c injector are considerably higher than those for the high P_c injectors. This is true for the data with film cooling as well as the data with no film cooling. Although the high and low P_c injectors were identical in design, other than the element hole sizes required to operate at different P_c levels, it should be noted that there are differences in the propellant momentum ratios between the two injectors. The absolute momentum of the liquid oxygen and the momentum ratio of the oxidizer to fuel are both higher with the high P_c injectors than with the low P_c injector. Since the high levels of heat transfer near the injector were attributed to injector recirculation, it is possible that the strength of the recirculation vortex is inversely proportional to the momentum ratios and may account for the difference in the correlation coefficient between the high and low P_c injectors near the injector face.

The other major difference between the high and low P_c data is the large spike in C_d at station 9 for the high P_c injector tests. Although there appears to be no ready explanation for the phenomenon, it is felt that this too may be injector related.

However, with the exception of station 9, the values of C_d for stations 7 to 19 are of the same magnitude at a given station and do not appear to be a function of the P_c range or the amount of peripheral film cooling. Thus, most of the data for the convergence, throat, and divergence sections of the thrust chamber appear to be characteristic of the geometric contour and should be applicable to the nuclear rocket.

Circumferential Effects

In reference 11 it was shown that a circumferential variation in the heat-transfer coefficient could be attributed to flow or O/F variations because of the use of a single inlet on the gaseous hydrogen injector manifold. Since each of the injectors used in the tests reported herein also had a single inlet on the manifold, a question arises as to what effect this might have on the data. The only configuration where this effect could be ascertained was that with the tests involving high P_c injector 1, where 2.28 percent cooling was injected around the entire outer periphery. Inspection of the data revealed that no circumferential effect on the heat-transfer coefficients resulted from the use of a single inlet on the injector manifold.

Correlation Using Re_x

A problem exists when using a correlation where the local diameter is the characteristic dimension in the Reynolds number. For example, heat-transfer coefficients calculated for the constant-diameter section of the chamber are constant for all locations. Since there is a region near the injector where there has been no boundary layer development, it is unreasonable to assume that the heat-transfer coefficient should be a constant for the entire constant-diameter section of the chamber. Therefore, in reference 11 the authors suggested that when using a correlation of the type $St^* Pr^{*-.7} = CRe^{*-.2}$ to calculate local heat-transfer coefficients for a rocket thrust chamber, the characteristic dimension in the Reynolds number should be the axial distance from the injector face. The supposition is that the boundary layer in a rocket thrust chamber, especially for high contraction ratios, develops in a manner more similar to flow on a flat plate and the heat transfer behaves similarly.

To show the effect of using the axial distance in the Reynolds number, the C_d values shown in figures 12(a) to (c) were recalculated and are shown as C_x's in figures 13(a) to (c). A comparison of figure 13(a) with figure 12(a) shows that the large peak value of C_d at station 2 with no cooling is reduced 37 percent when calculated as C_x. Similar effects are shown in figures 13(b) and (c).

The net effect of using axial distance in the Reynolds number is to reduce the value of C near the injector and increase the value of C downstream of the point where the axial distance from the injector face equals the local diameter. Figure 14 shows C_d and C_x as functions of axial distance for all the uncooled data. Each point represents the least squares fit of the data shown in figures 11(a) to (r) using the local diameter in the Reynolds number for the C_d values and axial distance for the C_x values. It can be seen that the magnitude of the axial variation in C_d is greatly reduced when calculated as C_x. The values of C_d vary from 0.056 near the injector to 0.017 just downstream of the throat to 0.019 at the last measuring station in the divergence section. However, the values of C_x vary from 0.0346 near the injector to 0.0214 upstream of the throat to 0.0231 at the last measuring station in the divergence section. Thus, correlating these data on a station by station basis using the Re_x method reduces the overall axial variation of the correlation coefficient by 66 percent.

Since correlating the data station by station on an Re_x basis reduces the axial variation in C, the next logical step is to ascertain what deviation would result about a single correlating line representing a fit of all the data taken collectively from all stations. This was done for the results reported herein and compared with the results of two other investigations.

In reference 11, two sets of data were shown where the Reynolds numbers in the Stanton-Prandtl groupings were based on the axial distance from the injector face. Fig-

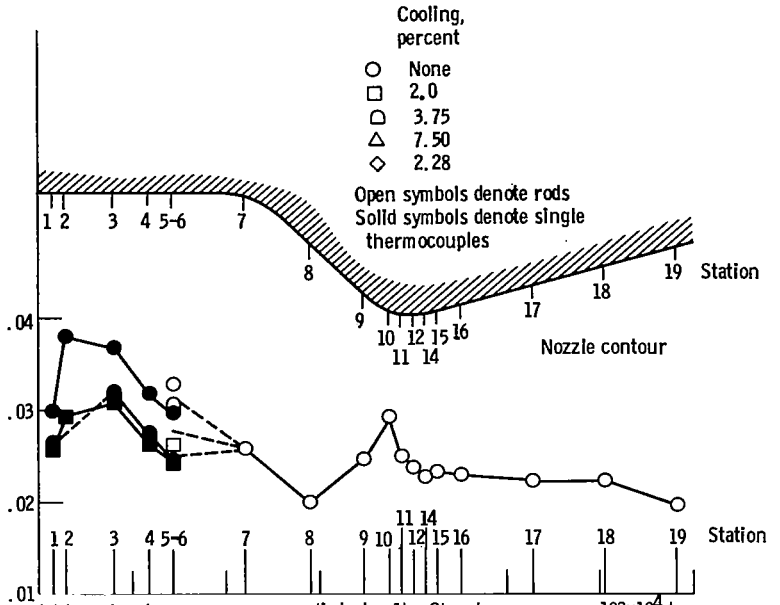

(a) Low chamber pressure range (injector 1). Chamber pressure, 103×10^4 to 286×10^4 newtons per square meter (150 to 415 psia).

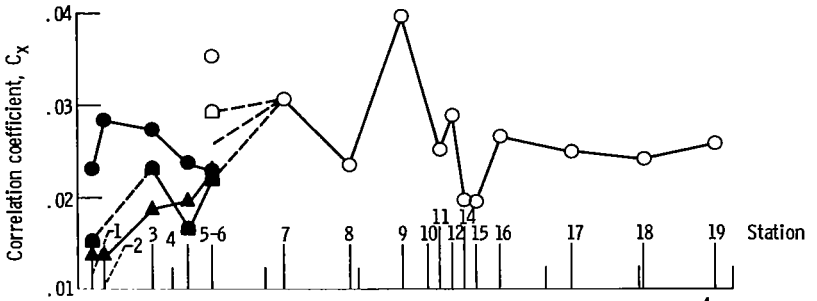

(b) High chamber pressure range (injector 2). Chamber pressure, 425×10^4 to 583×10^4 newtons per square meter (617 to 846 psia).

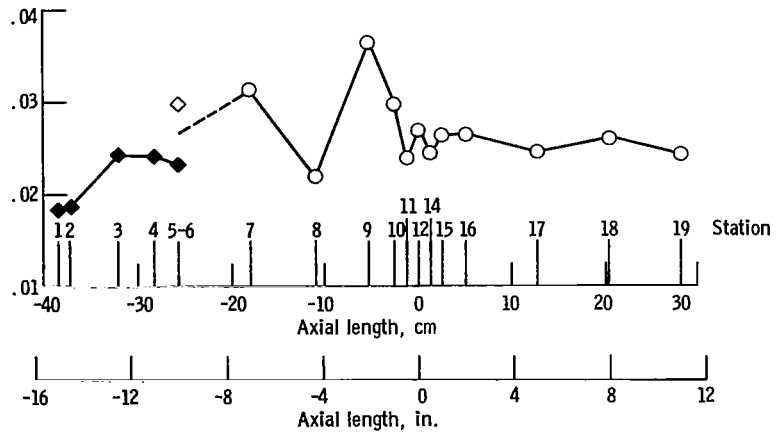

(c) High chamber pressure range (injector 3). Chamber pressure, 364×10^4 to 571×10^4 newtons per square meter (528 to 828 psia).

Figure 13. - Average correlation coefficients C_x as function of axial length for $St^* Pr^{*.7} = C_x Re_x^{*-.2}$.

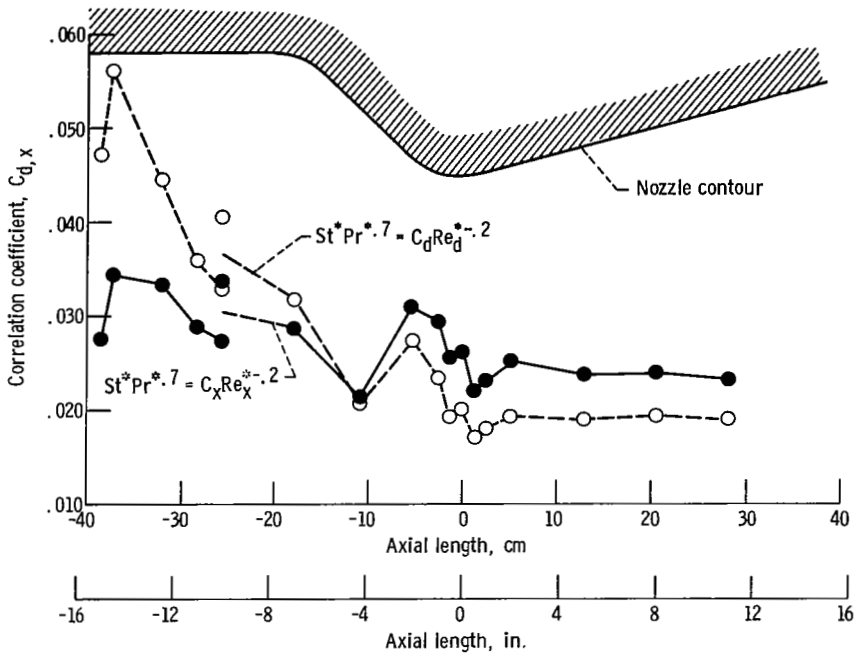

Figure 14. - Average C_d's and C_x's for all no cooling data.

ure 10 from reference 11 shows the data from the Lewis Research Center tests and figure 11 of reference 11 shows the data from the Jet Propulsion Laboratory tests. In these figures, a single correlating line and lines representing the $\pm 1.96\ \sigma$ variation about the correlation were shown for the two sets of data. In figure 15, all of the no cooling data of this investigation are shown as functions of Re_x. The solid symbols represent the data for stations 1 to 6. The $\pm 1.96\ \sigma$ lines for the data of reference 11 are also shown.

It can be seen that the data have about the same spread as shown by the $1.96\ \sigma$ lines of reference 11, but they lie at a somewhat higher level. In each case the use of Re_x makes the data lie fairly well along a line having a -.2 slope; however, the $1.96\ \sigma$ lines represent a spread of +33 to -40 percent about the mean. For some rocket thrust chamber designs, a correlation having this tolerance may be close enough; however, for more critical designs a refinement of the Re_x method of calculating heat-transfer coefficients appears to be warranted. Another approach to the design problem would be to use the Re_x method for the first portion of the thrust chamber and then to switch back to the use of the Re_d method, or to a boundary layer solution such as described in reference 12, for the remainder of the thrust chamber.

It is interesting to note that if one had used a flat plate correlation of the form

$$St^*Pr^{*.7} = 0.0295\ Re_x^{*-.2}$$

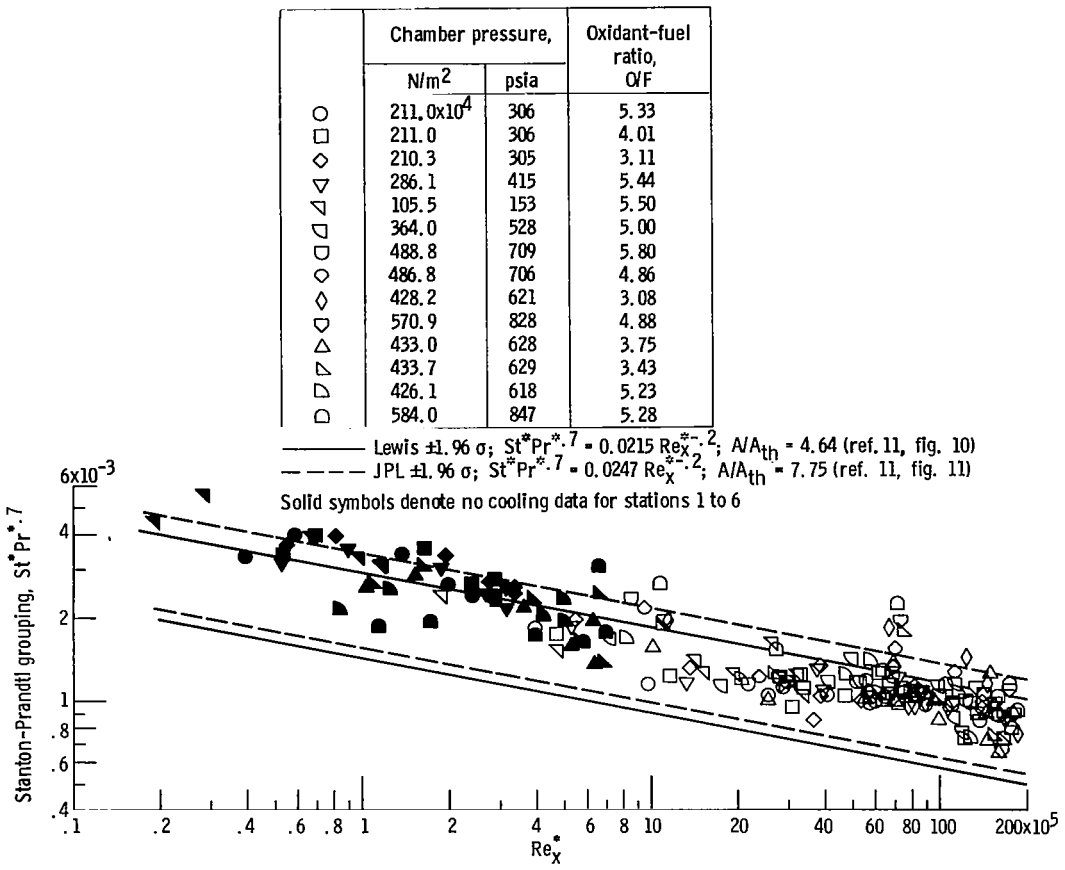

Figure 15. - All no cooling data as function of Reynolds number.

to predict the heat-transfer coefficients for the barrel section of the thrust chamber (the data for no cooling represented by the solid symbols in fig. 15) a good approximation of the heat-transfer coefficients would have resulted.

Recirculation Effects

As discussed earlier in the report, the results for no cooling revealed that unusually high heat-transfer coefficients were being encountered near the injector as evidenced by the high values of C_d in this region. This effect was more pronounced in the low chamber pressure range (fig. 12(a)) than in the high pressure range (fig. 12(b)). To more clearly demonstrate the magnitude of this phenomenon, typical values of q, T_{gw}, and h are shown for two runs with no cooling in figure 16. Figure 16(a) shows the data of run 11 and figure 16(b) shows the data of run 51. Both run conditions are at approximately

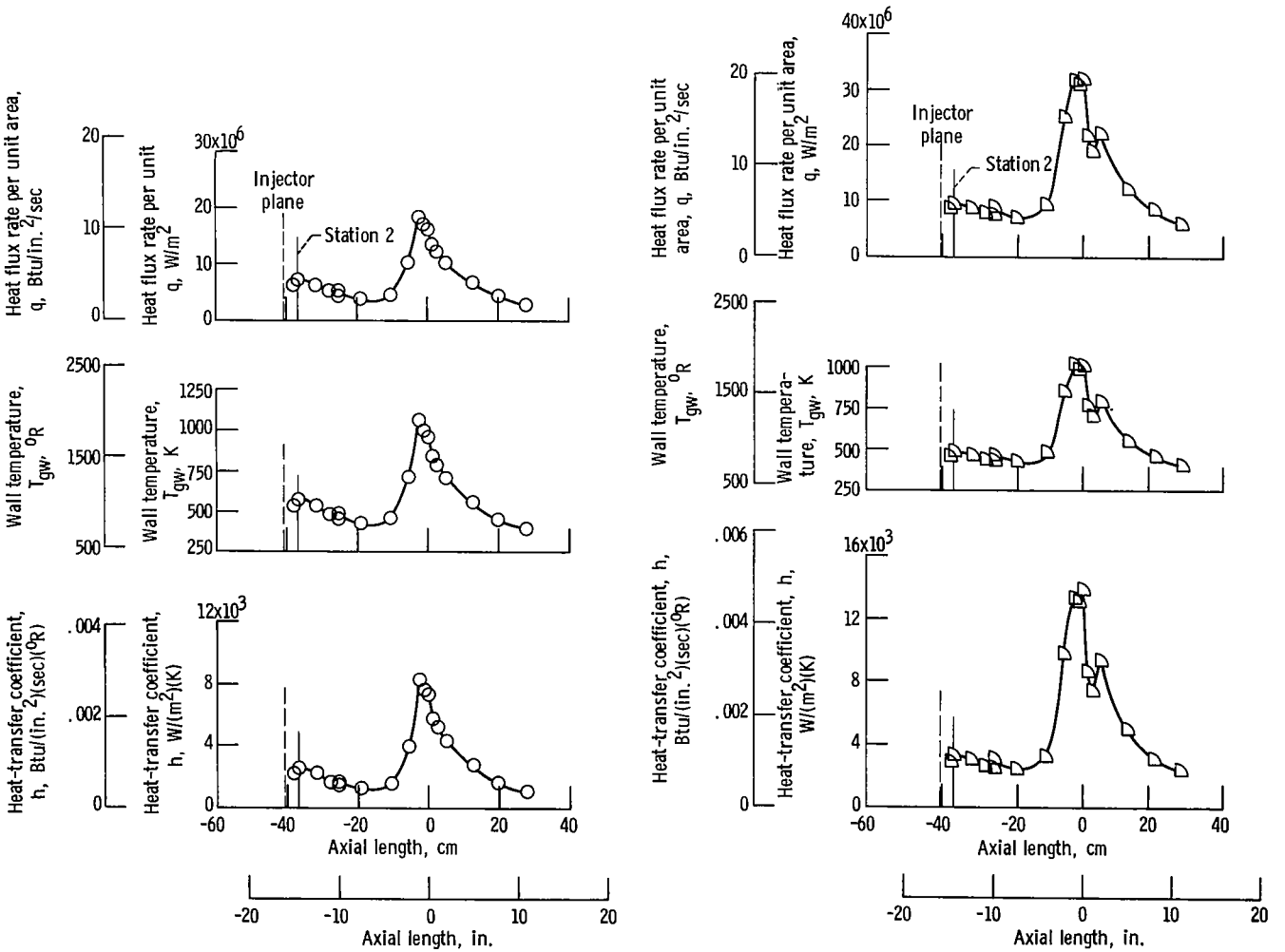

(a) Run 11. Chamber pressure, 211.0x10^4 newtons per square meter (306 psia); oxidant-fuel ratio, 5.33; no cooling.

(b) Run 51. Chamber pressure, 426.1x10^4 newtons per square meter (618 psia); oxidant-fuel ratio, 5.23; no cooling.

Figure 16. - Heat flux, wall temperature, and heat-transfer coefficient as functions of axial location.

the same O/F. It can be seen that the value of h at station 2 of run 11 is nearly equal to the value of h at station 2 of run 51, even though the chamber pressure of run 11 is one-half that of run 51. This suggests that a localized region of recirculation may be causing high values of h near the injector in the low P_c range. Evidence of this is shown in figure 17. This figure shows the burned out tubes of a liquid hydrogen cooled thrust chamber run with H_2-O_2 at a 206.8×10^4 newton per square meter (300 psia) chamber pressure. The low chamber pressure injector was used for this test with no peripheral film cooling. The thrust chamber had the identical geometric contour as the copper heat-sink thrust chamber used for the results reported herein. The damage appears to be typical of a recirculation problem and occurred at what would be station 2 of the copper thrust chamber.

The liquid cooled thrust chamber was designed in the constant diameter chamber section with a hot-gas-side correlation coefficient of $C_d = 0.031$. The coolant-side weight flow for the test run was that designed for operation at 206.8×10^4 newtons per square meter (300 psia). It is obvious that 0.031 was not a high enough correlation coefficient for that location in the thrust chamber. However, if the flat plate correlation

$$St^* Pr^{*\cdot 7} = 0.0295\ Re_x^{*-.2}$$

had been used to design the thrust chamber, the predicted h would have been 50 percent higher at station 2 than that predicted using the Re_d method. Although the flat plate correlation may not have predicted a high enough h to account for the recirculation effects

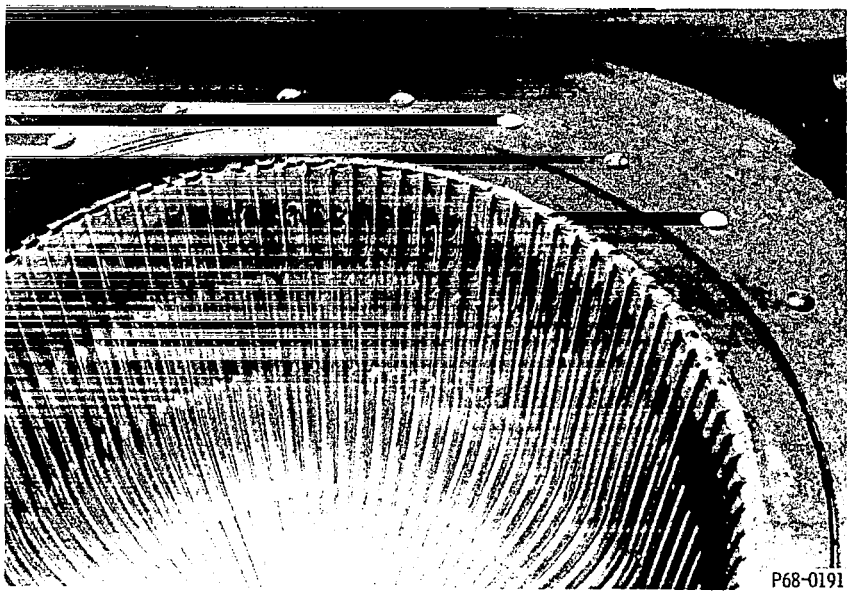

Figure 17. - Burnout of liquid hydrogen cooled thrust chamber.

in the low P_c range, it would have more than accounted for the high values of h in the high P_c range.

SUMMARY OF RESULTS

An experimental investigation was performed to obtain heat-transfer coefficients on a thrust chamber simulating the geometry of a nuclear rocket thrust chamber. The tests were performed with and without peripheral film cooling. The results for no film cooling are the following:

1. The average correlating coefficient C_d in

$$St^* Pr^{*\cdot 7} = C_d Re_d^{*-.2}$$

where St, Pr, and Re are the Stanton, Prandtl, and Reynolds numbers, varied from 0.056 (0.0381 m (1.5 in.) from the injector) to 0.017 (0.0127 m (0.5 in.) downstream of the throat) to 0.019 at the last measuring station of the divergence section.

2. When the local diameter in the Reynolds number was replaced by the axial distance from the injector face, the average correlating coefficient C_x varied from 0.0346 (0.0381 m (1.5 in.) from the injector) to 0.0214 (0.108 m (4.25 in.) upstream of the throat) to 0.0231 at the last measuring station of the divergence section. This was a reduction of 66 percent in the overall axial variation of the correlation coefficients.

3. The high heat-transfer coefficients near the injector, which were attributed to injector recirculation, could be approximated using the flat plate correlation

$$St^* Pr^{*\cdot 7} = 0.0295\ Re_x^{*-.2}$$

where the axial distance from the injector is the characteristic dimension in the Reynolds number.

The results for peripheral film cooling are as follows:

1. The average peak value of C_d (0.0381 m (1.5 in.) downstream of the injector) was reduced by 50 percent with 7.5 percent peripheral film cooling with an injector operating over a range of chamber pressures of 425×10^4 to 583×10^4 newtons per square meter (617 to 846 psia).

2. The average peak value of C_d (0.0381 m (1.5 in.) downstream of the injector) was reduced by an average of 25 percent for 2.0 percent and 3.75 percent peripheral cooling for an injector operating over a range of chamber pressures of 105.5×10^4 to 286×10^4 newtons per square meter (153 to 416 psia).

3. The effects of peripheral cooling dissipated before the convergence section of the thrust chamber.

CONCLUDING REMARKS

Other than a region near the injector where recirculation was present and a location upstream of the throat where an unexplainable spike in the heat-transfer coefficient was encountered, the data for the convergence, throat, and expansion regions are believed to be typical of the geometry and should be applicable to nuclear rocket thrust chambers.

Although the high level of heat transfer near the injector appeared to be due to injector recirculation, it is conceivable that similar characteristics are present in the nuclear thrust chamber where the gas issuing from discrete holes of the reactor core must expand into the large chamber region. Thus, it is probable that the heat-transfer coefficients for the nuclear thrust chamber are also varying from high to low in the barrel section.

When boundary layer solutions have been used to calculate heat-transfer coefficients for rocket thrust chambers, it has been common practice to start the calculation at the beginning of the convergence section. This leaves the designer in a quandary when it comes to calculating heat-transfer coefficients in the chamber. If one were to use the correlation $St^{*} Pr^{*\cdot 7} = 0.026\ Re_{d}^{*-.2}$, it would not account for a varying h due to recirculation or an undeveloped boundary layer, as this equation implies a constant h for the constant diameter chamber section. However, the Re_x method of computing h does give a varying h in the constant diameter portion of the nozzle, although one must know the correlation coefficient which applies. Based on the results reported herein, the flat plate correlation $St^{*} Pr^{*\cdot 7} = 0.0295\ Re_{x}^{*-.2}$ would give an approximation of the heat-transfer coefficients for the chamber region.

The film cooling results indicated that 2.0 percent cooling was somewhat more effective than 3.75 percent cooling for the low chamber pressure injector tests, and that 3.75 percent cooling was more effective than 7.5 percent cooling at some locations for the high chamber pressure injector 2 tests. Thus, it would appear that the optimum cooling has not been established for these configurations. Since the objective of film cooling is to reduce the heat flux to the wall at critical locations in the thrust chamber with the minimum loss in performance, any design using film cooling would require determination of the optimum cooling flow.

Other investigators have discovered the presence of high heat-transfer coefficients in the barrel section of high contraction ratio - high contraction angle thrust chambers; thus, more film cooling investigations should be conducted on this kind of configuration. Investigations should also be conducted to determine whether the use of discrete cooling

holes has an advantage over the use of a cooling ring, since the injection of coolant directly at a critical hot spot region might require less coolant than that injected by a cooling ring, thereby minimizing the performance losses.

Lewis Research Center,
National Aeronautics and Space Administration
Cleveland, Ohio, October 12, 1971,
112-29.

REFERENCES

1. Boldman, Donald R.; Schmidt, James F.; and Gallagher, Anne K.: Laminarization of a Turbulent Boundary Layer as Observed from Heat-Transfer and Boundary-Layer Measurements in Conical Nozzles. NASA TN D-4788, 1968.
2. Boldman, Donald R.; Neumann, Harvey E.; and Schmidt, James F.: Heat Transfer in 30° and 60° Half-Angle of Convergence Nozzles with Various Diameter Uncooled Pipe Inlets. NASA TN D-4177, 1967.
3. Reshotko, Meyer; Boldman, Donald R.; and Ehlers, Robert C.: Heat Transfer in a 60° Half-Angle of Convergence Nozzle with Various Degrees of Roughness. NASA TN D-5887, 1970.
4. Back, L. H.; Massier, P. F.; and Gier, H. L.: Convective Heat Transfer in a Convergent-Divergent Nozzle. TR-32-415, Jet Propulsion Lab., California Inst. Tech. (NASA CR-57326), Feb. 15, 1965.
5. Back, L. H.; Massier, P. F.; and Cuffel, R. F.: Flow Phenomena and Convective Heat Transfer in a Conical Supersonic Nozzle. J. Spacecraft Rockets, vol. 4, no. 8, Aug. 1967, pp. 1040-1047.
6. Schacht, Ralph L.; Quentmeyer, Richard J.; and Jones, William L.: Experimental Investigation of Hot-Gas Side Heat-Transfer Rates for a Hydrogen-Oxygen Rocket. NASA TN D-2832, 1965.
7. Carslaw, Horatio S.; and Jaeger, J. C.: Conduction of Heat in Solids. Second ed., Oxford University Press, 1959, pp. 304-306.
8. Storm, M. L.: Heat Conduction in Simple Metals. J. Appl. Phys., vol. 22, no. 7, July 1951, pp. 940-951.
9. Eckert, E. R. G.; and Drake, Robert M., Jr.: Heat and Mass Transfer. Second ed., McGraw-Hill Book Co., Inc., 1959.

10. Bartz, D. R.: A Simple Equation for Rapid Estimation of Rocket Nozzle Convective Heat Transfer Coefficients. Jet Propulsion Lab., California Inst. Tech., 1957, pp. 49-51.

11. Schacht, Ralph L.; and Quentmeyer, Richard J.: Axial and Circumferential Variations of Hot-Gas-Side Heat-Transfer Rates in a Hydrogen-Oxygen Rocket. NASA TN D-6396, 1971.

12. Ellicott, David G.; Bartz, Donald R.; and Silver, Sidney: Calculation of Turbulent Boundary-Layer Growth and Heat Transfer in Axisymmetric Nozzles. TR-32-387, Jet Propulsion Lab., California Inst. Tech., Feb. 15, 1963, p. 270.

NASA-Langley, 1972 —— 33 E-6553